Climatic Change (2019) 155:437–454
https://doi.org/10.1007/s10584-019-02475-w

Changes in vegetation and surface water balance at basin-scale in Central China with rising atmospheric CO_2

Richao Huang[1,2] · Xi Chen[3] · Qi Hu[4]

Received: 13 July 2018 / Accepted: 3 June 2019 / Published online: 21 June 2019
© Springer Nature B.V. 2019

Abstract
Elevated atmospheric CO_2 concentration alters vegetation growth and composition, increases plant water use efficiency (*WUE*), and changes surface water balance. These changes and their differences between wet and dry climate are studied at a mid-latitude experiment site in the Loess Plateau of China. The study site, the Jinghe River basin (JRB), covers an area of 43,216 km^2 and has a semiarid climate in the north and a semi-humid climate in the south. Two simulations from 1965 to 2012 are made using a site-calibrated Lund–Potsdam–Jena dynamic global vegetation model: one with the observed rise of the atmospheric CO_2 from 319.7–391.2 ppmv, and the other with a fixed CO_2 at the level of 1964 (318.9 ppmv). Analyses of the model results show that the elevated atmospheric CO_2 promotes growth of woody vegetation (trees) and causes a 6.0% increase in basin-wide net primary production (*NPP*). The *NPP* increase uses little extra water however because of higher *WUE*. Further examination of the surface water budget reveals opposite CO_2 effects between semiarid and semi-humid climates in the JRB. In the semiarid climate, plants sustain growth in higher CO_2 because of the higher level of intracellular CO_2 and therefore *WUE*, thus consuming more water and causing a greater decrease of surface runoff than in the fixed-lower CO_2 case. In the semi-humid climate, *NPP* also increases but by a smaller amount than in the semiarid climate. Plant transpiration (E_T) and total evapotranspiration (E) decrease in the elevated CO_2 environment, yielding the increase of runoff. This asymmetry of the effects of elevated atmospheric CO_2 exacerbates drying in the semiarid climate and enhances wetness in the semi-humid climate. Furthermore, plant *WUE* (=*NPP*/E_T) is found to be nearly invariant to climate but primarily a function of the atmospheric CO_2 concentration, a result suggesting a strong constraint of atmospheric CO_2 on biophysical properties of the Earth system.

1 Introduction

The atmospheric CO_2 concentration has been rising and is expected to continue rising through this century at a debatable rate. Elevated CO_2 concentration enhances the atmospheric

✉ Xi Chen
xichen@hhu.edu.cn

Extended author information available on the last page of the article

greenhouse effect and can cause changes in surface temperature and distribution of precipitation. Those changes could further result in shifts in distributions of global vegetation (e.g., Emanuel et al. 1985; Smith et al. 1992). Meanwhile, elevated atmospheric CO_2 stimulates the photosynthesis rate and increases carbon intake and assimilation by plants, thereby promoting plant growth (e.g., Prior et al. 2011). Increased photosynthesis rate would be accompanied by changes in plant transpiration rate. The latter can cause changes in water budget in soils and at the surface (e.g., Gerten et al. 2004). Idso and Brazel (1984) show that in an atmosphere of doubled CO_2 from its current amount, vegetation in the western United States would reduce transpiration by about two thirds of its current rate. This reduction of transpiration could result in an increase of streamflow by about 40–60%. Such changes in soil and surface water availability would further feedback to and influence ecological processes, such as phenological dynamics (Band et al. 1993) and water use efficiency (Winner et al. 2004; Yu et al. 2004). It is critical to understand these changes in vegetation–hydrology interactions in order to accurately describe future water resource availability and vegetation distribution in an elevated CO_2 environment (e.g., Arora 2002; Shafer et al. 2015; Sitch et al. 2008).

Responses of vegetation growth to elevated CO_2 amounts differ among plant species because of their different photosynthesis pathways (e.g., Miles et al. 2004; Prior et al. 2011). Miles et al. (2004) indicate that among all 69 Angiosperm species in the Amazonia, high trees (>25 m in height) exhibit the least response to changes in CO_2 amount, and species with narrow ranges and short generation times have the greatest response. Prior et al. (2011) show that plants with the C3 photosynthetic pathway often exhibit greater growth responses to CO_2 change than C4 plants. Elevated atmospheric CO_2 reduces plant transpiration by reducing stomatal aperture. This effect could be offset however by an increase in surface area of leaves for plants that grow faster in high CO_2 environment. These changes affect water budget at the surface and in soils. As Li and Ishidaira (2012) have shown, an increase in atmospheric CO_2 alone could lead to 11.9–21.8% runoff increase in humid areas (non-limited water environment) but to a huge 48.6% decrease in arid areas (water limited environment). Between humid and arid climates, ecological systems in semi-humid or semiarid climates are much more fragile, and the responses of vegetation dynamics and water balance to elevated CO_2 could be quite different from that in either humid or arid climate.

One such typical semiarid environment is in the Loess Plateau in central China. Historical records indicate that the Loess Plateau endured large alternations of warm-humid and cold-dry climate at various timescales (Tan et al. 2014). In the past 2000 years, the area has suffered a steady decline of forest coverage when its climate has become more semiarid. Corresponding changes in surface vegetation type, including vegetation loss in some areas, have raised the region's vulnerability to soil erosions and frequent extreme climate events, such as droughts and dust storms (Wang et al. 2006). It is interesting to know if this deteriorating situation might be altered by elevated atmospheric CO_2 and the impacts of elevated CO_2 on vegetation and surface hydrology. Such information is essential for making policies to revive or improve local environmental integrity (Xiao 2015).

The increase of the atmospheric CO_2 concentration in the Loess Plateau has been at a rate of 2.2 ± 0.8 ppmv a^{-1} from 1991 to 2011 (e.g., Zhou et al. 2003; Fang et al. 2014). This rate is higher than the average global rate of 1.69 ppmv a^{-1} (MacFarling Meure et al. 2006), and could strongly affect vegetation and its interactions with hydrology in the Loess Plateau.

In this study, we quantify the effect of increasing CO_2 on vegetation and surface hydrology in the Loess Plateau, using the Jinghe River basin in the Plateau as our study site. We use the Lund–Potsdam–Jena (LPJ) dynamic global vegetation model to quantify vegetation responses

in different CO_2 change scenarios. The effects of change in vegetation function in the elevated CO_2 environment on surface water balance will be quantified. In addition, differences of those effects in semiarid and semi-humid climate conditions in the Loess Plateau will be examined to understand variations of the effects of elevated CO_2 in different climates.

2 Study area and data

The Jinghe River is one of the main tributaries of the Yellow River in China. Jinghe River Basin is in the central Loess Plateau in northwestern China from 106°14′–109°06′E and 34°46′–37°24′N, covering an area of 45,373 km^2. The area of the basin upstream of the hydrological station (basin drainage outlet) at Zhangjiashan is 43,216 km^2 (Fig. 1a) and is the focus area of this study (hereafter JRB). The average elevation of the JRB is 1424 m above sea level.

From the recent survey data of Peng et al. (2015), the JRB has 46.5% grassland, 41.6% farmland, and 10.2% forest. Forests are concentrated in semi-humid climate areas in the south and along the slopes of terrains in the southeast of the JRB (Fig. 1a and b). The northern portion of the JRB is dry and featured with loess tableland with grass and shrubs as the dominant vegetation. Over the recent history of agricultural development, suitable areas in the basin have been cultivated to grow crops, resulting in nearly 42% of crop lands in the JRB (Suo et al. 2008).

Data used in our vegetation (LPJ) model include monthly meteorological data from 1916 to 2012. These data are from the CRU TS3.23 dataset (Harris et al. 2014) and include monthly precipitation, mean temperature, rainy day frequency, and cloud cover, all at 0.5°×0.5° resolution. Because the CRU data underestimates the precipitation and overestimates the temperature of the JRB (Huang et al. 2016), we adjust the CRU data based on a local 0.5°×0.5° resolution gridded dataset, CN05, which was developed by the China Meteorological Administration. The CN05 dataset, developed from observations at more than 2472 stations in China, has an advantage in data accuracy, but covers a shorter period from 1961 to 2012. We used the 52-year CN05 data and developed their linear correlations with the CRU TS3.23 data of monthly precipitation and temperature at the same grids. Using those relationships, we adjusted the CRU monthly precipitation and temperature data from 1916 to 2012. We note that this adjustment could add uncertainties to the climate data used in this study. Effects of these potential uncertainties on our model outcomes would be expected to be small however because of very high correlations between the two datasets in their shared decades ($R^2 = 0.896$ for precipitation and 0.996 for temperature).

Analyzing the data from 1916 to 2012, we found that the JRB averaged annual precipitation is 520.7 mm. Annual precipitation decreases from the southeast semi-humid area (annual mean of 589.5 mm) to the northwest semiarid area (annual mean of 428.9 mm) (Fig. 1b). The driest year is 1942, and the wettest year is 1964 (346.0 and 760.2 mm annual precipitation averaged in the JRB, respectively) (Fig. 2a). The mean annual temperature in the JRB decreases from the southeast semi-humid area (ranging from 6.2–12.3 °C) to the northwest semiarid area (ranging from 5.4–8.2 °C) (Fig. 1c). The annual mean temperature fluctuates between 6.8 and 9.7 °C. It is warmer before the 1950s and also after 1986 and cooler from 1950 to 1985 (Fig. 2b).

Annual atmospheric CO_2 concentration data developed by the Scripps CO_2 Program (MacFarling Meure et al. 2006) are used in this study. The data show that the annual

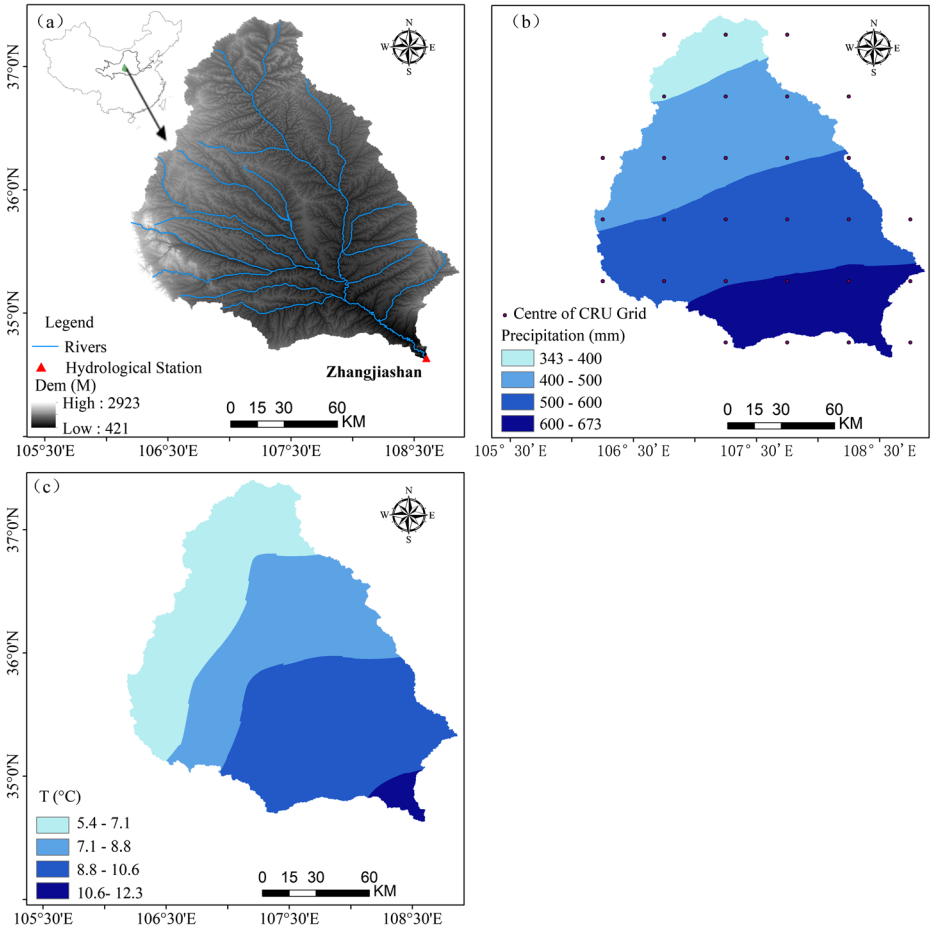

Fig. 1 Distributions of (a) topography, (b)mean annual precipitation, and (c) mean annual temperature in the JRB, China

mean atmospheric CO_2 concentration in the study region rose from 301.6 ppmv in 1916 to 391.2 ppmv in 2012. The rise has accelerated since 1965 (Fig. 2c), especially from 1991 to 2010 when the CO_2 concentration jumped from 353.2 to 387.0 ppmv. These changes are consistent with the observed rise from 355.2 to 389.5 (±1.9) ppmv measured at the international CO_2 monitoring site in Waliguan (100.9°E, 36.28°N) near the JRB (Fang et al. 2014; Zhou et al. 2003).

Monthly streamflow data from 1932 to 2012 at the Zhangjiashan hydrological station are obtained from the Shanxi Hydrometric and Water Resource Bureau and used in comparison with the LPJ model output. Remote sensing products of vegetation in JRB derived from the Global Inventory Modeling and Mapping Studies (GIMMS) NDVI (Normalized Difference Vegetation Index) (1982–2012) and from the MODIS MOD15A2H-LAI (leaf area index) (2005–2012) are used to compare with modeled vegetation conditions. The soil profile data used in the model are from the Food and Agriculture Organization (FAO) soil dataset (Zobler 1986) with nine soil types.

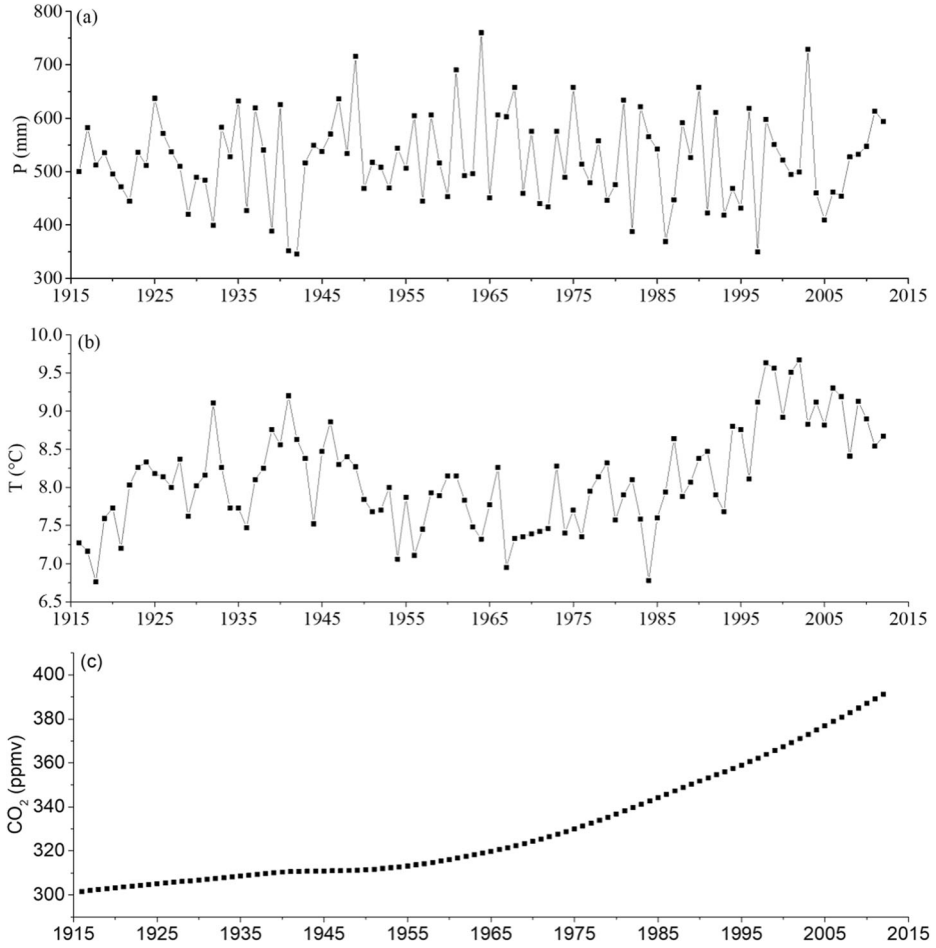

Fig. 2 Variations in (a) annual precipitation (P), (b) annual average surface air temperature (T), and (c) annual CO_2 concentration from 1916 to 2012 in JRB

3 Lund–Potsdam–Jena model, model validation, and experimental design

The Lund–Potsdam–Jena (LPJ) dynamic global vegetation model is a process-based approach to describe terrestrial vegetation dynamics and associated carbon and water exchanges in the terrestrial system. Details of model physics, biophysics, and dynamics are described in Sitch et al. (2003) and Gerten et al. (2004) and not repeated here.

Calibration of the LPJ model in the JRB follows the procedures described in Sitch et al. (2003). The model was integrated using data from the JRB. The data include observed climate, soils, and atmospheric CO_2 concentration in the JRB averaged over the first 30 years of our study period, 1915–2012. The integration was for 1000 years to allow various carbon pools in soils and terrestrial carbon cycle that are not observed at the site to reach an equilibrium (Sitch et al. 2003). This process also yields vegetation type and composition in the JRB consistent

with its climate and soils. Only at such an equilibrium could the model be used to examine responses of carbon cycle, including vegetation and hydrology dynamics, to anthropogenic and climate disturbances.

The model was further validated by comparisons of water balance between simulated and observed runoff and vegetation between simulated LAI and satellite remote sensing NDVI/LAI. In our calibration/validation, we found that the thickness of the two soil layers in the LPJ model is the most sensitive parameter influencing the model results. Our calibration suggests the same thicknesses of 1.4 m for both the soil layers in the study basin. Other model parameters suitable for the JRB are found to be similar to those suggested by Sitch et al. (2003). Details of the calibration are summarized in Huang et al. (2016).

The calibrated LPJ model simulated dominant vegetation type and distribution are shown in Fig. 3 and are consistent with that observed in the JRB (vegetation classification scheme of Prentice et al. (2011) is used in this study). In Fig. 3, temperate broad-leaved summer-green (TBS) is in the southeast of the JRB. Northward of that area, grass (C3) becomes dominant and is mixed with shrubs and patches of short woody plants/trees (mostly boreal needle-leaved evergreen, BNE), before becoming grass only in the northern tip of the JRB. This pattern largely resembles the actual land-cover (contoured areas numbered 1–4 in Fig. 3) that has TBS in the southeast JRB, more grass mixed with shrubs in the main body of the basin, and grass only in its northern tier. The major differences in model simulated and actual land-cover are along the east fringes of the JRB, where the dominant BNE and BBS (boreal broad-leaved summer-green) plant types along the slopes of terrains are not simulated as the dominant plant types. Because in those areas the model also has BNE and BBS in the vegetation mix but as lesser dominant types than grass, these differences in model simulated vegetation in the JRB are considered small and acceptable.

The calibrated LPJ model with the land-cover is used to simulate JRB runoff from 1965 to 2012. (Our production integration is from 1965 to 2012 because the atmospheric CO_2 concentration before 1965 remains similar to the value used in the calibration, 1915–1945.) Comparisons of runoff between the simulation and observation at the Zhangjiashan hydrological station (outlet of the JRB) show that the coefficient of determination (R^2) is 0.36 for annual runoff (Fig. 4a) and $R^2 = 0.7$ for average monthly runoff (Fig. 4b); both significant at the 99% confidence level. While the statistics of the simulated runoff are strong, there are some large deficiencies between the simulated and actual runoff. For example, the simulated annual runoff loses strong interannual fluctuations shown in the observed runoff in some periods (Fig. 4a). The average annual hydrograph from the simulation has more runoff in spring months and also a near one-month delay in peak runoff (Fig. 4b). These differences could affect model results related to those particular aspects and, because of such, they should be interpreted with caution.

While comparing annual variations of simulated LAI with observed NDVI from 1982 to 2012 and available LAI from 2005 to 2012 (Fig. 5), we found that they match well during 1982–1994 and 2005–2012. Relatively large discrepancies exist from 1995 to 2004 primarily because of changes of cultivated areas in the JRB resulting from regional economic policy changes. In the mid-1990s, farmers were given the freedom to migrate to cities to find jobs, and many of them did. That migration affected land-cover in the following years. Part of those farmers returned to their farms to receive subsidies when a "Grain for Green" policy was initiated in 1999. In subsequent years, that policy resulted in an increase of woody vegetation in some previous farm lands (Geng et al. 2008).

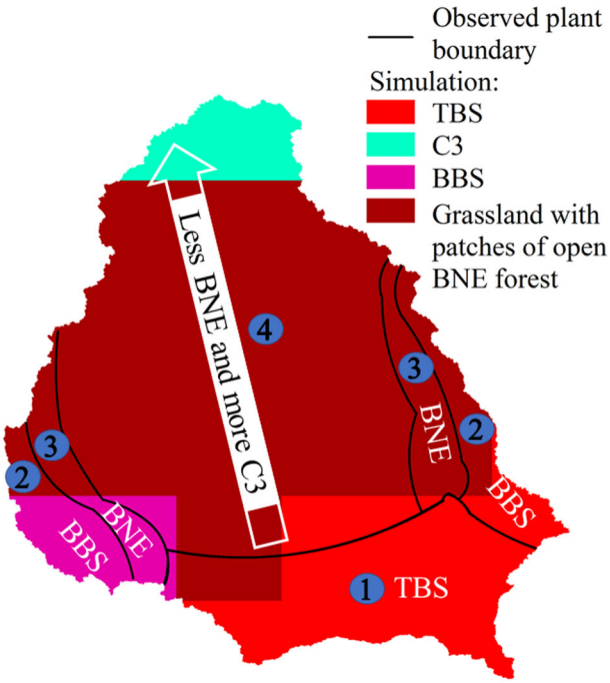

Fig. 3 Color code shows PFTs simulated by the LPJ model. Contour lines show the boundaries of the observed land cover types with the region 4 for grass mixed with crops

After these calibration and validation, we apply the LPJ model to the JRB to study basin-scale vegetation and water balance responses to the rising CO_2 amount in the atmosphere. Two model experiments are carried out. Both are integrated from 1965 to 2012 because most of the CO_2 increase took place after 1965 (Fig. 2c) when the climate data are also most reliable. One experiment uses the LPJ model to simulate vegetation dynamics and interactions with water balance at a fixed-lower CO_2 concentration in the atmosphere. The fixed-lower CO_2 amount is 318.9 ppmv, observed in 1964. The other uses the observed rate of increase in atmospheric CO_2 concentration from 1965 to 2012. Because climate conditions in these experiments are identical, their differences in vegetation condition and water balance in JRB will help distinguish effects of the rising concentration of atmospheric CO_2.

4 Effects of elevated CO_2 on vegetation dynamics and water balance

In evaluating the effects of elevated atmospheric CO_2 on vegetation and surface water balance, we use model simulated plant characteristics, e.g., LAI, foliage projected cover (*FPC*), and net primary production (*NPP*, gross primary production less respiration cost). Among model outputs of hydrological variables used in our analyses are monthly and annual runoff and actual evapotranspiration (E), which is the sum of plant transpiration (E_T), bare soil evaporation (E_S), and evaporation of plant intercepted water (E_I). The average of any of these variables over the JRB is calculated using the grid areal weighted averaging method.

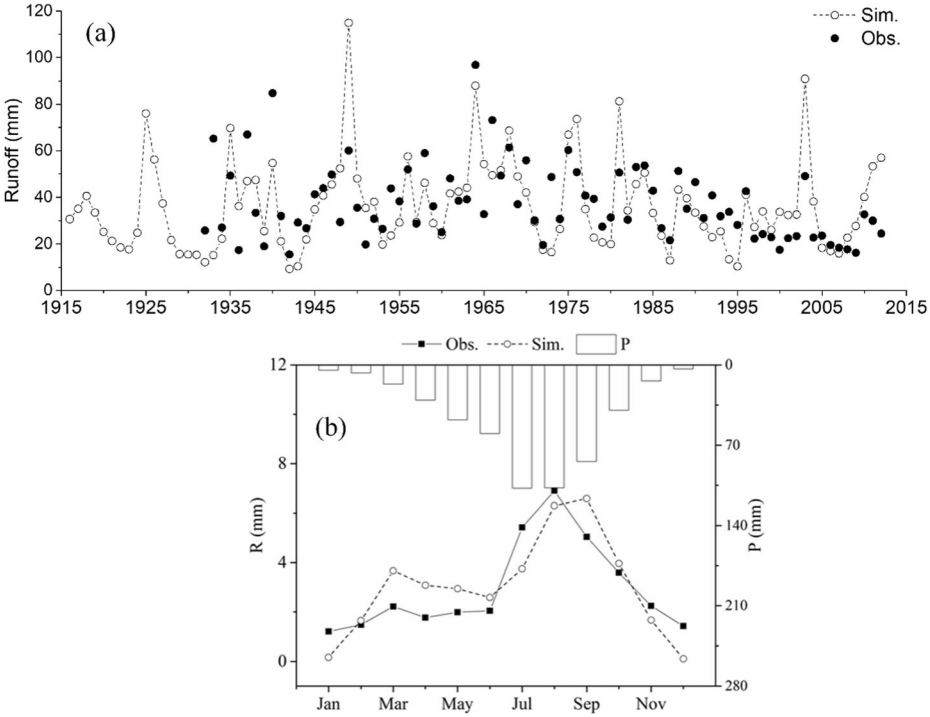

Fig. 4 Observed and (a) simulated annual runoff and (b) 1965–2012 averaged monthly runoff of JRB. Annual precipitation is shown in (b) by the scale on the right axis

4.1 Basin-averaged effects of elevated CO_2 in 1965–2012

Model results summarized in Table 1 show that following the rising atmospheric CO_2 from 1965 to 2012 trees are becoming more dominant than grass in the land-cover of the JRB. This change is evident in that *LAI*, *FPC*, and *NPP* increase for TBS, BNE, and BBS, but decrease for C3 (grass). Compared to the results of model simulation using fixed-lower CO_2, the basin average annual *LAI*, *FPC*, and *NPP* increase by 8.4, 0.7, and 6.0%, respectively (Table 1). The time series of *NPP* and annual *E* and runoff (*R*) are shown in Fig. 6b–d for the rising CO_2 and

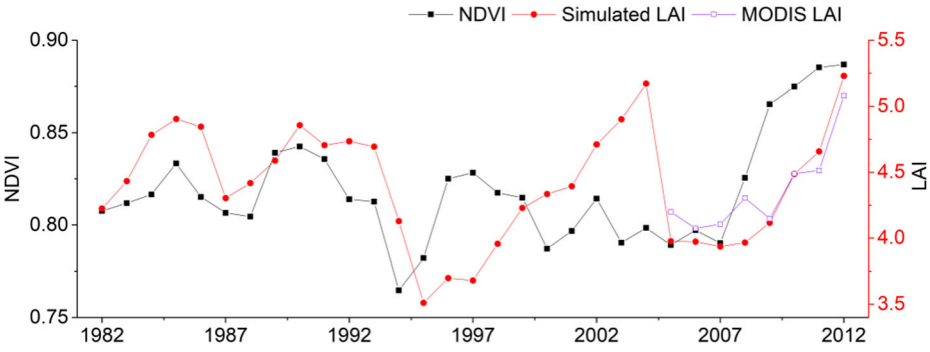

Fig. 5 Simulation of leaf area index (*LAI*) and observation from GIMMS-NDVI and MODIS-LAI satellite production

Table 1 Mean annual vegetation and water balance indicators of the JRB from the two simulations (1965–2012). Average values for the semiarid and semi-humid area of the JRB are also included. [relative difference = (rising CO_2 – fixed-lower CO_2)/ fixed-lower CO_2]

Variables		Entire basin			Semiarid region (P≤500 mm)			Semi-humid region (P≥500 mm)		
		Rising CO_2	Fixed-lower CO_2	Relative difference (%)	Rising CO_2	Fixed-lower CO_2	Relative difference (%)	Rising CO_2	Fixed-lower CO_2	Relative difference (%)
LAI	TBS	3.91	3.57	9.7	1.89	1.60	18.1	5.28	4.89	7.8
	BNE	5.58	5.22	6.7	5.48	5.10	7.5	5.64	5.31	6.2
	BBS	4.11	3.68	11.7	2.30	1.87	23.0	5.32	4.89	8.8
	C3	0.29	0.34	−15.6	0.45	0.54	−16.7	0.18	0.21	−14.0
	Average	3.47	3.20	8.4	2.53	2.28	11.1	4.10	3.83	7.3
FPC (%)	TBS	34.2	33.7	1.5	2.7	2.3	16.9	55.4	54.7	1.3
	BNE	39.3	37.8	4.0	70.1	66.6	5.3	18.7	18.4	1.6
	BBS	11.9	11.3	5.3	5.6	4.9	15.5	16.0	15.7	1.8
	C3	12.1	14.0	−13.6	17.4	20.3	−14.3	8.5	9.8	−13.5
	Sum	97.5	96.8	0.7	95.8	94.1	1.8	98.7	98.7	0.0
NPP (gCm^{-2})	TBS	194.4	182.3	6.6	11.3	9.3	21.5	317.5	298.5	6.4
	BNE	163.3	147.9	10.4	290.3	260.4	11.5	78.0	72.4	7.7
	BBS	67.8	61.8	9.7	28.6	23.5	21.7	94.2	87.5	7.7
	C3	71.8	77.2	−7.0	85.1	92.7	−8.2	62.8	66.7	−5.8
	Sum	497.3	469.2	6.0	415.3	385.9	7.6	552.5	525.1	5.2
E (mm)	E_T	347.7	350.0	−0.7	291.5	290.1	0.5	385.5	390.3	−1.2
	E_S	64.6	67.5	−4.3	52.9	59.7	−11.4	72.4	72.8	−0.5
	E_I	72.9	68.3	6.7	76.2	70.3	8.4	70.7	67.0	5.5
	Sum	485.2	485.8	−0.1	420.6	420.1	0.1	528.6	530.1	−0.3
R (mm)		36.5	35.9	1.7	17.9	18.5	−3.2	48.9	47.7	2.5

fixed-lower CO_2 simulations. The difference of *NPP* between the two simulations enlarges following the rise of atmospheric CO_2 (Fig. 6b). For example, from 2000 to 2012, the mean annual *NPP* of the JRB increases by 10.6% from *NPP* in the fixed-lower CO_2 case (Table 2).

Figure 6b also shows that while *NPP* increases following the rise of atmospheric CO_2, the fluctuation of *NPP* follows the variation of local climate, especially precipitation (cf. Fig. 6b and a). This result indicates that although a richer CO_2 environment encourages plant growth by increasing photosynthetic uptake, the actual growth in individual years is still dependent on water availability (precipitation). The climate limitation on *NPP* is caused by stomata closure of plants in response to drier climate. While this process reduces plant water loss, it slows plant photosynthetic uptake of CO_2. As shown in Drake et al. (2017), however, this latter effect can be offset to some extent by the increase of internal CO_2 partial pressure. Such effect is also evidenced in our result (upper histogram in Fig. 6b) by the larger relative difference of *NPP* in dry climate.

Compared to the strong response of *NPP*, the response of surface water balance to rising atmospheric CO_2 is small (cf. Fig. 6b–d). This weak sensitivity of water balance to rising CO_2 results from some cancellations among different processes contributing to E in the elevated CO_2 environment. Specifically, a decrease of E_S and an increase of E_I (Fig. 7b and c) contribute to an increase in vegetation growth and thus higher *LAI* and *FPC*. Plant transpiration E_T decreases in most years but increases in some very dry years. These are suggested by the positive differences of E_T in Fig. 7a when compared to the fixed-lower CO_2 case. The change of E_T further amplifies with rising atmospheric CO_2. In the LPJ model, E_T is determined from

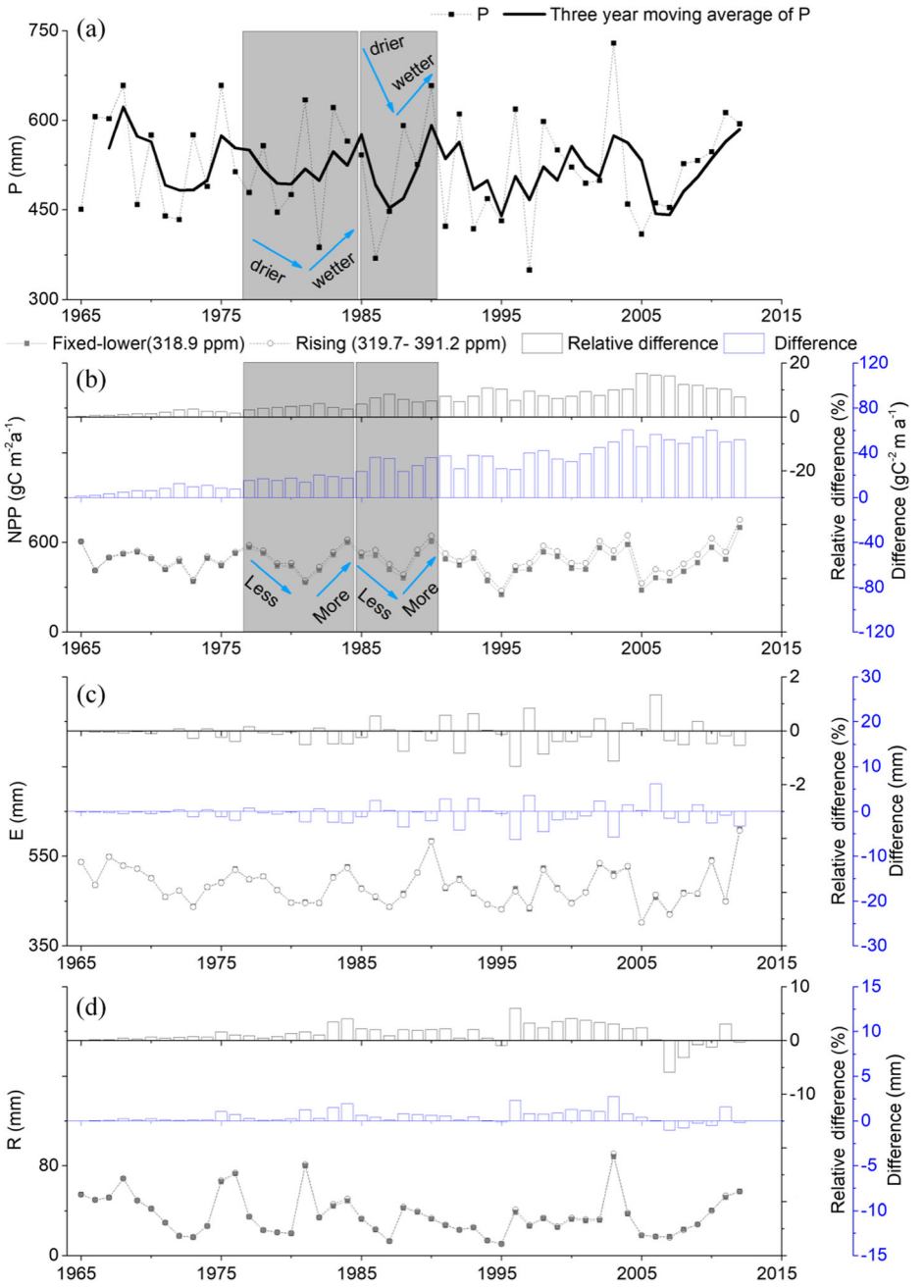

Fig. 6 Three-year moving average of (a) observed precipitation (P), (b) simulated *NPP*, (c) actual evapotranspiration (*E*), and (d) runoff (*R*) for the rising (dash-line) and fixed-lower CO_2 (gray-line) cases. Blue and black histograms show, respectively, difference and relative difference between the rising CO_2 and fixed-lower CO_2 results. Theshaded area indicates the two periods (1977–1984 and 1985–1990) used in the detailed analysis

Table 2 The same as Table 1 but for results averaged over 2000–2012

Variables		Entire basin			Semiarid region (P≤500 mm)			Semi-humid region (P≥500 mm)		
		Rising CO_2	Fixed-lower CO_2	Relative difference (%)	Rising CO_2	Fixed-lower CO_2	Relative difference (%)	Rising CO_2	Fixed-lower CO_2	Relative difference (%)
LAI	TBS	3.91	3.32	17.8	1.90	1.41	34.8	5.26	4.60	14.3
	BNE	5.32	4.67	13.9	4.80	4.09	17.4	5.67	5.06	12.1
	BBS	4.12	3.33	23.7	2.26	1.47	53.7	5.37	4.59	17.0
	C3	0.35	0.47	−25.5	0.64	0.88	−27.3	0.16	0.19	−15.8
	Average	3.43	2.95	16.3	2.40	1.96	22.4	4.11	3.61	13.9
FPC (%)	TBS	34.9	34.2	2.0	2.9	2.3	26.1	56.4	55.7	1.3
	BNE	37.1	33.3	11.4	64.7	55.8	15.9	18.6	18.1	2.8
	BBS	12.3	11.4	7.9	6.1	4.6	32.6	16.5	16.0	3.1
	C3	12.5	16.2	−22.8	20.0	26.9	−25.7	7.4	9.0	−17.8
	Sum	96.9	95.1	1.9	93.7	89.5	4.7	99.0	98.8	0.2
NPP (gCm^{-2})	TBS	207.0	186.8	10.8	12.6	9.2	37.0	337.5	306	10.3
	BNE	160.5	130.6	22.9	278.5	218.3	27.6	81.3	71.7	13.4
	BBS	73.0	61.2	19.3	31.8	21.1	50.7	100.7	88.2	14.2
	C3	78.8	91.1	−13.5	105.7	130.3	−18.9	60.7	64.8	−6.3
	Sum	519.3	469.7	10.6	428.6	378.9	13.1	580.2	530.7	9.3
E (mm)	E_T	350.9	354.0	−0.9	290.4	285.9	1.6	391.5	399.8	−2.1
	E_S	63.9	70.1	−8.8	59.8	74.1	−19.3	66.6	67.4	−1.2
	E_I	70.0	61.2	14.4	67.6	55.4	22.0	71.6	65.1	10.0
	Sum	484.7	485.3	−0.1	417.8	415.4	0.6	529.7	532.2	−0.5
R(mm)		36.9	36.4	1.4	17.8	20.0	−11.0	49.7	47.4	4.9

$E_T = \mathrm{Min}[S, D] \times f_v$. In this formula, S is plant- and soil-limited water supply function, and D is an atmosphere-controlled demand function that is a strong function of potential canopy conductance (Federer 1982). The parameter f_v is the fraction of vegetation cover in a grid cell. In the well-watered condition ($D < S$), E_T decreases in the elevated CO_2 environment because of a decrease in canopy conductance (g_c) (Gerten et al. 2004). In water-limit condition ($D \geq S$), E_T increases in the elevated CO_2 environment primarily because of an increase in vegetation coverage (f_v) at higher rates of photosynthesis (Keenan et al. 2013).

Our simulated results show that from 1965 to 2012, the averaged annual E_T in the JRB deceased by 2.3 mm (−0.7%) in the rising atmospheric CO_2 simulation compared to the fixed-lower CO_2 run. This decrease of E_T is a net result of a decrease in grass E_T (−6.9 mm) and an increase in E_T from woody vegetation (trees) (4.6 mm), when grass (C3) shifts to trees (TBS, BNE, and BBS) in the elevated CO_2 environment. The decreased E_T from grass is contributed by decreases of 6.3 and 0.6 mm (91.3 and 8.7% of the decreased E_T) due to decreases in vegetation coverage (f_v) and canopy conductance (g_c), respectively. The increased E_T from trees is contributed by increases of 3.2 and 1.4 mm (69.6 and 30.4% of the increased E_T) due to increases in vegetation coverage (f_v) and canopy conductance (g_c), respectively. These changes indicate negative and positive g_c responses to elevated atmospheric CO_2 for grass and trees in the study region. Increases of g_c in an elevated CO_2 environment have also been reported in hot and dry biomes in dry environments (Purcell et al. 2018).

Meanwhile, E_S decreases from 1965 to 2012 by 4.3%, and E_I increases by 6.7% in the JRB (Table 1). Together, these changes result in a slight decrease of E in the rising atmospheric CO_2 simulation compared to the fixed-lower CO_2 run. Consistent with this slightly reduced E, mean

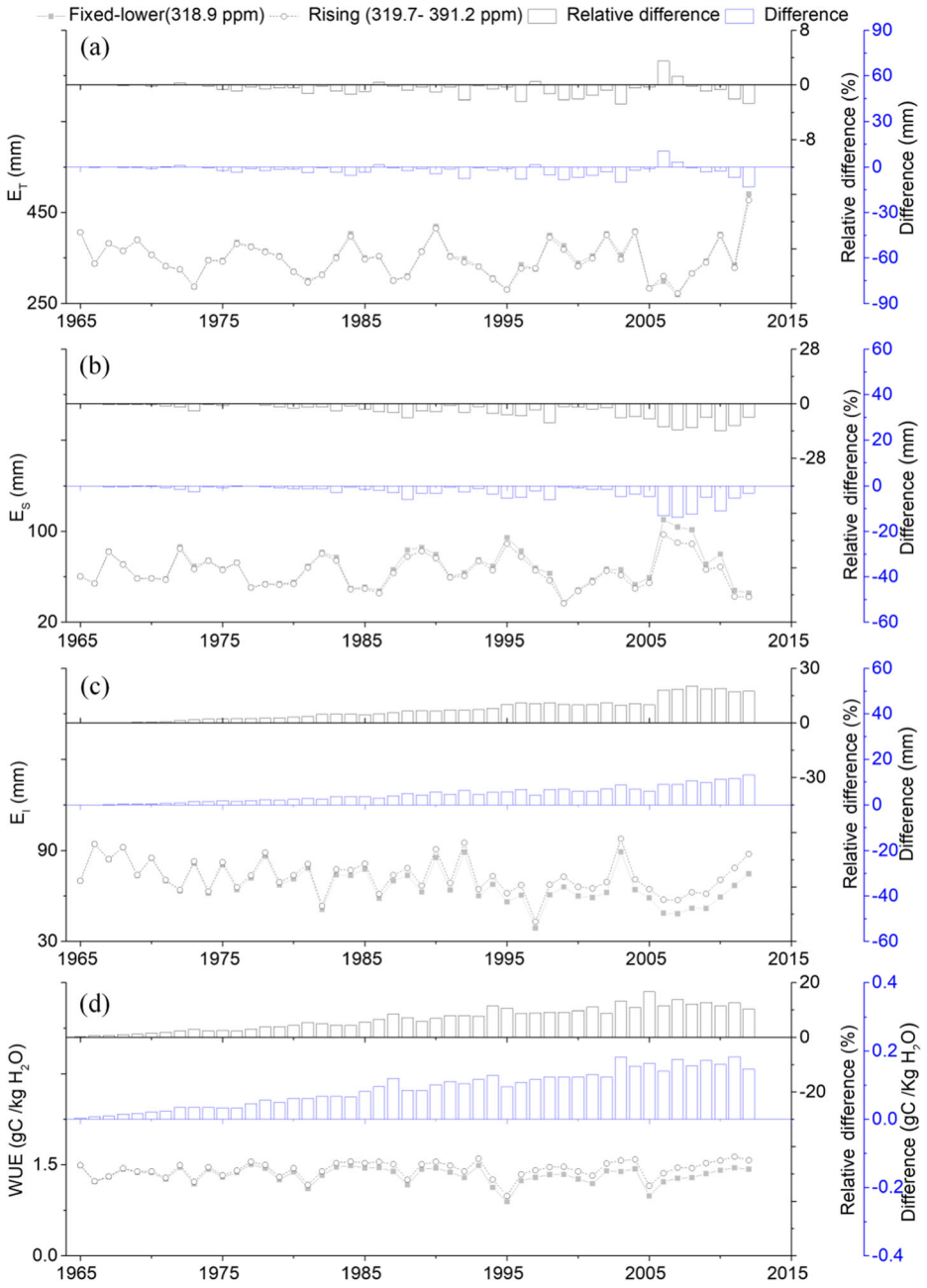

Fig. 7 Simulated annual values of (a) E_T, (b) E_S, (c) E_I, and (d) *WUE* for the rising CO_2 (dash-line) and fixed-lower CO_2 (gray-line). Blue and black histograms show, respectively, the difference and relative difference between the rising CO_2 and fixed-lower CO_2 results

annual runoff *R* increases slightly with the rise of atmospheric CO_2. The average increase of *R* is 1.7% relative to the fixed-lower CO_2 case (Table 1). We also note large fluctuations of *R* especially in dry years. In those years, increased water consumption by vegetation growth in

the elevated CO_2 environment causes R to decrease. As an example, in the dry year of 2007 simulated R is 5.8% lower in the elevated CO_2 case than the fixed-lower CO_2 case (Fig. 6d).

4.2 Effects of elevated CO_2 in semiarid and semi-humid areas in the JRB

We further examine variations of the response of vegetation and surface water balance to rising atmospheric CO_2 across different climate zones in the JRB. On the basis of the strong north-south precipitation gradient (Fig. 1b), we divide the JRB into a semiarid region north of the 500 mm annual precipitation contour line (the boundary between the blue and light blue zones in Fig. 1b) and a semi-humid region south of that line. In addition, we compare the responses of water use efficiency WUE ($WUE = NPP/E_T$) in these two climate regions. It is noted that because the climate variables driving the LPJ model are the same in the rising CO_2 and fixed-lower CO_2 simulations, no indirect effect of CO_2 rise on these responses through its effect on the climate is measured.

Table 1 summarizes the responses of LAI, NPP, E, and R to the rising atmospheric CO_2 from 1965 to 2012 in the semiarid region of the JRB. Compared to the results from the fixed-lower CO_2 simulation, NPP and LAI in the elevated CO_2 run show an increase of 7.6 and 11.1%, respectively, in the semiarid region. This increase is limited to tree species, i.e., TBS, BNE, and BBS, however. The largest increase is seen in BNE (more drought resistance species) and the smallest in TBS. NPP and LAI of C3 (grass) decrease in the elevated CO_2 case. Because the decrease in C3 is small, the averaged NPP and LAI increase in the semiarid region.

An intriguing difference in the semiarid region is between the large increase in LAI and NPP and rather small changes in E in response to the rise of atmospheric CO_2 (Table 1). In fact, the mean of annual E changes little between the rising CO_2 and fixed-lower CO_2 cases. The small changes in E is a net result of quite different responses of the components constituting E, i.e., E_I, E_T, and E_S, in their responses to the CO_2 increase. In Table 1, E_I shows a considerable increase in the rising CO_2 case. This increase could result from expansion of woody (tree) vegetation (BNE, BBS, and TBS) in the elevated CO_2 environment. Consistently, evaporation from bare surfaces, E_S, is 11.4% lower in the rising CO_2 than in the fixed-lower CO_2 case. These changes nearly offset one another, thus yielding a rather small net positive change in E, which also explains a slight reduction of R in the semiarid region of the JRB following the rise of CO_2.

Changes of these vegetation and water budget components and their net effects in the semi-humid region of the JRB are also summarized in Table 1. Results in Table 1 show a 5.2% increase of NPP in the rising CO_2 case from the NPP of the fixed-lower CO_2 case. This amount of increase is smaller than the increase of 7.6% in the semiarid region (Table 1). The increase of NPP in the semi-humid region in the rising CO_2 case is also attributed to an expansion of tall woody vegetation and small contraction of C3 plants. Furthermore, from analyzing the NPP budget, we find that the responses of BNE and BBS to rising CO_2 is mild. A large change is found in TBS species (Table 1). The net increase of NPP in the semi-humid region is smaller than in the semiarid region with the same rising CO_2 rate because, according to Miles et al. (2004) and Tricker et al. (2009), the short rotation species, BNE as well as C3, in the semiarid region are more sensitive to the rising atmospheric CO_2 than trees of TBS and BBS in the semi-humid region (also see the distribution of plant functional types in Fig. 3).

Total evapotranspiration E in the semi-humid region is slightly smaller in the rising CO_2 case than in the fixed-lower CO_2 case because of reduced E_T and E_S. The reduction of E_T is particularly large. The reduced E explains the slight increase of R in the semi-humid region of the JRB (Table 1).

The differences of surface water balance and vegetation growth between the semiarid and semi-humid regions are amplified in a higher CO_2 environment. As shown in Table 2, for the average value during 2000–2012 when the atmospheric CO_2 concentration rose to the highest in the study period, the increase of *LAI* and *NPP* in the rising CO_2 case are larger in the semiarid area (22.4 and 13.1%, respectively, relative to the fixed-lower CO_2 case) than in the semi-humid area (13.9 and 9.3%, respectively). The stimulated plant growth in the high CO_2 environment consumes more water (0.6% increase of E and 11% decrease of R) in the semiarid region. Less water is used in the semi-humid area (0.5% decrease of E and 4.9% increase of R).

The changes of *NPP* and E_T caused by rising CO_2 define the change of water use efficiency, $WUE(=NPP/E_T)$. Our further analysis reveals a constraint of CO_2 on those changes such that *WUE* remains nearly invariant in the semi-humid and semiarid climate regions under the same CO_2 level. In the rising atmospheric CO_2 case, the average *WUE* over 1965–2012 is 1.43 gC/kg H_2O in both sub-climate regions. The same *WUE* of 1.34 gC/kg H_2O is also obtained in the two different sub-climate regions in the fixed-lower CO_2 case (Table 3). Additional evaluations of the *NPP* and E_T data averaged in the recent higher CO_2 concentration period from 2000 to 2012 show a higher but still constant $WUE = 1.48$ gC/kg H_2O across the different climate regions in the JRB. It may be particularly intriguing that *WUE* remains near the constant of 1.34 gC/kg H_2O in those years for the fixed-lower CO_2, as in the prior years in the fixed CO_2 run, even when the climate input has changed considerably. These results, summarized in Table 3, suggest that plant *WUE* would increase primarily following the rise of the atmospheric CO_2 concentration, while climate effects are on interannual fluctuations of plant growth and E_T. Those changes are, as suggested by our results, kept near a constant *WUE* specified by the atmospheric CO_2 concentration: less *NPP* in drier years with proportionally reduced E_T and more *NPP* and E_T in wetter years (Figs. 6a, b, and 7a). Higher *WUE* in elevated atmospheric CO_2 is attributed to smaller E_T in the semi-humid region, and it is attributed to larger E_T in the semiarid climate (E_T is smaller/larger in the elevated CO_2 than in the fixed-lower CO_2 for the semi-humid/semiarid climate area, as shown in Table 3). Higher *WUE* with increase in E_T has also been found at three FLUXNET sites (Keenan et al. 2013).

Table 3 Mean annual *NPP*, E_T, and *WUE* for the period of 1965–2012 and 2000–2012

Parameter	Period	Entire basin		Semiarid region		Semi-humid region	
		Rising CO_2	Fixed-lower CO_2	Rising CO_2	Fixed-lower CO_2	Rising CO_2	Fixed-lower CO_2
NPP (gC m^{-2})	1965–2012	497.3	469.2	415.3	385.9	552.5	525.1
	2000–2012	519.3	469.7	428.6	378.9	580.2	530.7
E_T (mm)	1965–2012	347.7	350.0	291.5	290.1	385.5	390.3
	2000–2012	350.9	354.0	290.4	285.9	391.5	399.8
$WUE = NPP/E_T$	1965–2012	1.43	1.34	1.42	1.33	1.43	1.35
(gC/kg H_2O)	2000–2012	1.48	1.33	1.48	1.33	1.48	1.33

5 Discussions and concluding remarks

Rising atmospheric CO_2 concentration stimulates plant photosynthesis while often, but not always, reducing plant stomatal aperture and conductance (e.g., Saxe et al. 1998; Farquhar 1977). The subsequent increase in carbon uptake and assimilation by a plant enhances its growth and water use efficiency. These processes would affect the growth of plants and can further cause changes in vegetation composition and consequently the surface water balance. In this study, we examined these changes in the Jinghe River Basin (JRB) in the Loess Plateau of central China, using the Lund–Potsdam–Jena (LPJ) dynamic global vegetation model. After calibrating and validating the model to the JRB, we analyzed our model results from two simulations, both from 1965 to 2012: one using the observed rise in atmospheric CO_2 amount and the other using a fixed lower CO_2 concentration observed in 1964.

Results from analyses of the model simulated data show a significant increase in vegetation growth in the JRB from 1965 to 2012 following the rising atmospheric CO_2 concentration. The average *NPP* and *LAI* are 10.6 and 16.3%, respectively, higher in the rising atmospheric CO_2 simulation than the fixed-lower CO_2 run, averaged over 2000–2012 when the CO_2 level is the highest in recent decades (average 379 ppmv). While these results reiterate the enhanced fertilization effect of elevated atmospheric CO_2 on vegetation growth (e.g., Prior et al. 2011; Swann et al. 2016), additional effects of rising atmosphere CO_2 are found to change the vegetation composition in the JRB. Our results indicate an increase of woody (tree) vegetation (more dominant among grid cell vegetation species) and a decrease of C3 (grass) following the rise of atmospheric CO_2.

The basin averaged change of water budget between the two simulations shows a slight decrease in total evapotranspiration, E, and an increase in runoff, R, in the elevated CO_2 run in the study period (1965–2012). Further examinations of individual terms in the budget of E (which is a major source/sink for R) reveal that plant transpiration E_T generally decreases following the rise of atmospheric CO_2, a result suggesting an increase in plant water use efficiency (*WUE*) in an elevated CO_2 environment. This model result is consistent with prior findings (e.g., Gerten et al. 2004) and is attributed to shifts of grass (C3) to trees (TBS, BNE, and BBS) in an elevated CO_2 environment.

Our further examinations of vegetation dynamics and surface water budget in semiarid versus semi-humid climate areas in the JRB indicate some opposite CO_2 effects. We found that in elevated atmospheric CO_2 condition plants can sustain growth in a semiarid (water-limited) climate. This is because, as shown in Drake et al. (2017), a higher level of intracellular CO_2 may mitigate the effects of droughts and reduce the effect of aridity on some plants through increased *WUE*. As a result, plants would consume more water in a drier climate of elevated atmospheric CO_2 and enhance the decrease of surface runoff. The mean annual runoff decreases by 11.0% (relative to the runoff in the fixed-lower CO_2 case) in the semiarid area of the northern JRB in the high CO_2 concentration condition from 2000 to 2012.

On the other hand, in the semi-humid region of the southern JRB, the *NPP* also increases in the elevated CO_2 case but at a rate smaller than in the semiarid north. E_T and total surface evapotranspiration E decrease slightly compared to the fixed-lower CO_2 case. This decrease leads to a small increase of the runoff in the semi-humid climate, in contrast to the decrease of runoff in the semiarid climate in the elevated CO_2 environment. This asymmetry of the effects of elevated atmospheric CO_2 could have exacerbated surface drying in the semiarid climate, while enhancing surface wetness in the semi-humid climate.

An increase of *WUE* (=NPP/E_T) has been a known result of rising atmospheric CO_2 (e.g., Keenan et al. 2013), although its cause remains in debate. While early experiments emphasized the effects of either an increase in *NPP* or a decrease in E_T on *WUE* of various plant species (e.g., Gunderson et al. 1993; Rogers et al. 1994), recent studies have shared the consensus that the increase of plant *WUE* in an elevated CO_2 environment results from CO_2 effects on both *NPP* and E_T (e.g., Keenan et al. 2013). Our analysis of the asymmetry of the rising CO_2 effect on amplifying extreme hydrological conditions in dry and wet climate indicates that an increase in *WUE* primarily follows the rise of atmospheric CO_2, and it is not sensitive to wet or dry climate in our study region. This result suggests a biophysical constraint of the atmospheric CO_2 concentration on plant growth and Earth's vegetation environment and offers a plausible explanation of increasing extreme conditions in the climate of fast rising atmospheric CO_2.

It is recognized that our result of a nearly invariant *WUE* in semiarid and semi-humid climates under a given atmospheric CO_2 concentration and underlined biophysical and phenological processes are derived from this one study basin and based on a single (LPJ) model. Limitations of the LPJ model, particularly in its absence of groundwater and topographic effects (e.g., loess tables and gullies in the JRB) on re-distribution of soil moisture and lateral flows, pose uncertainties on the validity of this constraint and applicability of certain results from this study. These results need to be further validated in regions of different latitude, longitude, and climate, and by more advanced dynamic vegetation models before being proven as biophysical properties of the Earth system.

Acknowledgements We thank two anonymous reviewers of an early version of this work for their suggestions and comments that have helped improve the clarity of this presentation. This research was supported by the National Key Research and Development Program of China (2017YFC0406101) and the UK-China Critical Zone Observatory (CZO) Program (41571130071). Qi Hu was supported by USDA Cooperative Research Project NEB-38-088.

References

Arora V (2002) Modeling vegetation as a dynamic component in soil-vegetation-atmosphere transfer schemes and hydrological models. Rev Geophys 40:3-1-3-26

Band LE et al (1993) Forest ecosystem processes at the watershed scale: incorporating hillslope hydrology. Agric For Meteorol 63:93–126

Drake BL et al (2017) The carbon fertilization effect over a century of anthropogenic CO_2 emissions: higher intracellular CO_2 and more drought resistance among invasive and native grass species contrasts with increased water use efficiency for woody plants in the US southwest. Glob Chang Biol 23(2):782–792

Emanuel WR, Shugart HH, Stevenson MP (1985) Climate change and the broad-scale distribution of terrestrial ecosystem complexes. Clim Chang 7:29–43

Fang SX et al (2014) In situ measurement of atmospheric CO_2 at the four WMO/GAW stations in China. Atmos Chem Phys 14:2541–2554

Farquhar GD (1977) Stomatal function in relation to leaf metabolism and environment. Symp Soc Exp Biol 121: 471–505

Federer CA (1982) Transpirational supply and demand: plant, soil, and atmospheric effects evaluated by simulation. Water Resour Res 18:355–362

Geng Y et al (2008) Temporal and spatial distribution of cropland-population-grain system and pressure index on cropland in Jinghe watershed. Trans Chin Soc Agric Eng 24(10):68–73

Gerten D et al (2004) Terrestrial vegetation and water balance—hydrological evaluation of a dynamic global vegetation model. J Hydrol 286:249–270

Gunderson C et al (1993) Foliar gas exchange responses of two deciduous hard woods during 3 years of growth in elevated CO2: no loss of photosynthetic enhancement. Plant Cell Environ 16:797–797

Harris I et al (2014) Updated high-resolution grids of monthly climatic observations - the CRU TS3.10 dataset. Int J Climatol 34(3):623–642
Huang R et al (2016) Validation of watershed soil effective depth based on water balance and its effect on simulation of land surface water-carbon flux. Acta Geograph Sin 71:807–816
Idso SB, Brazel AJ (1984) Rising atmospheric carbon dioxide concentrations may increase streamflow. Nature 312:51–53
Keenan TF et al (2013) Increase in forest water-use efficiency as atmospheric carbon dioxide concentrations rise. Nature 499(7458):324
Li Q, Ishidaira H (2012) Development of a biosphere hydrological model considering vegetation dynamics and its evaluation at basin scale under climate change. J Hydrol 412-413:3–13
MacFarling Meure C et al (2006) Law dome CO_2, CH_4 and N_2O ice core records extended to 2000 years BP. Geophys Res Lett 33:70–84
Miles L, Grainger A, Phillips O (2004) The impact of global climate change on tropical forest biodiversity in Amazonia. Glob Ecol Biogeogr 13:553–565
Peng H et al (2015) An eco-hydrological model-based assessment of the impacts of soil and water conservation management in the Jinghe River Basin, China. Water 7:6301–6320
Prentice IC et al (2011) Modeling fire and the terrestrial carbon balance. Glob Biogeochem Cycles 25:GB3005
Prior SA et al (2011) Review of elevated atmospheric CO_2 effects on plant growth and water relations: implications for horticulture. Hortsci A Publ Am Soc Horticult Sci 46:54–62
Purcell C et al (2018) Increasing stomatal conductance in response to rising atmospheric CO_2. Ann Bot 121: 1137–1149
Rogers H et al (1994) Plant responses to atmospheric CO_2 enrichment with emphasis on roots and the rhizosphere. Environ Pollut 83:155–189
Saxe H et al (1998) Tree and forest functioning in an enriched CO_2 atmosphere. New Phytol 139:395–436
Shafer SL et al (2015) Projected future vegetation changes for the Northwest United States and Southwest Canada at a fine spatial resolution using a dynamic global vegetation model. PLoS One 10:e0138759
Sitch S et al (2003) Evaluation of ecosystem dynamics, plant geography and terrestrial carbon cycling in the LPJ dynamic global vegetation model. Glob Chang Biol 9:161–185
Sitch S et al (2008) Evaluation of the terrestrial carbon cycle, future plant geography and climate-carbon cycle feedbacks using five dynamic global vegetation models (DGVMs). Glob Chang Biol 14:2015–2039
Smith TM et al (1992) Modeling the potential response of vegetation to global climate change. Adv Ecol Res 22: 93–98
Suo A et al (2008) Vegetation deficiency in a typical region of the loess plateau in China. Bot Stud 49:57–66
Swann AL et al (2016) Plant responses to increasing CO_2 reduce estimates of climate impacts on drought severity. Proc Natl Acad Sci U S A 113:10019
Tan L et al (2014) Cyclic precipitation variation on the western loess plateau of China during the past four centuries. Sci Rep 4:6381
Tricker P et al (2009) Water use of a bioenergy plantation increases in a future high CO_2 world. Biomass Bioenergy 33(2):200–208
Wang L et al (2006) Historical changes in the environment of the Chinese loess plateau. Environ Sci Pol 9:675–684
Winner WE et al (2004) Canopy carbon gain and water use: analysis of old-growth conifers in the Pacific northwest. Ecosystems 7:482–497
Xiao J (2015) Satellite evidence for significant biophysical consequences of the "grain for green" program on the loess plateau in China. J Geophys Res Biogeosci 119:2261–2275
Yu G-R, Wang Q-F, Zhuang J (2004) Modeling the water use efficiency of soybean and maize plants under environmental stresses: application of a synthetic model of photosynthesis-transpiration based on stomatal behavior. J Plant Physiol 161:303–318
Zhou L et al (2003) Background variations of atmospheric carbon dioxide and its stable carbon isotopes at Mt.Waliguan. Acta Sci Circumst 5:295–300
Zobler L (1986) A world soil file for global climate modeling. Nasa TM-87802. National Aeronautics and Space Administration, Washington, D.C.

Publisher's note Springer Nature remains neutral with regard to jurisdictional claims in published maps and institutional affiliations.

Affiliations

Richao Huang [1,2] · Xi Chen [3] · Qi Hu [4]

[1] State Key Laboratory of Hydrology-Water Resources and Hydraulic Engineering, Hohai University, Nanjing 210098, China

[2] College of Hydrology and Water Resources, Hohai University, Nanjing 210098, China

[3] Institute of Surface-Earth System Science, Tianjin University, Tianjin 300072, China

[4] School of Natural Resources and Department of Earth and Atmospheric Sciences, University of Nebraska-Lincoln, Lincoln, NE 68583, USA